Journal Name

ARTICLE

Insights into the durability of Co-Fe spinel oxygen evolution electrocatalysts via *operando* studies of catalyst structure

Received 00th January 20xx,
Accepted 00th January 20xx

DOI: 10.1039/x0xx00000x

www.rsc.org/

L. Calvillo[a,*], F. Carraro[a], O. Vozniuk[b], V. Celorrio[c,§], L. Nodari[d], A. E. Russell[e], D. Debellis[f], D. Fermin[c], F. Cavani[b], S. Agnoli[a] and G. Granozzi[a]

Elemental reorganisation and oxidation state changes of key active sites in Co-Fe spinels are investigated by *in situ* X-ray photoemission spectroscopy (XPS) and *operando* X-ray absorption spectroscopy (XAS) under oxygen evolution operating conditions. The combination of the two techniques allow to identify both the surface and bulk modifications on the oxides and relate them to the activity loss during extended cycling. The results show that Co-Fe spinels experience a surface irreversible phase evolution under oxygen evolution reaction (OER) conditions, resulting in the formation of an amorphous layer composed of new stable Co(III) and Fe(III) species. Accelerated ageing tests show that the durability, intended as the performance loss during cycling treatments, is not directly related to the structural/chemical stability of the spinels but to the new species formed at the surface due to the electrochemical work. Thus, the material that experienced more significant changes was also the most durable one, demonstrating that the understanding of the chemical and/or structural evolution of the materials during the catalytic process can be the key for the design of highly active and stable catalysts.

1 Introduction

The production of hydrogen driven by renewable energy, through the water splitting (WS) process performed in electrolysers powered by photovoltaic cells, is a key process in the development of a more sustainable energy economy. However, this process is limited by the high overpotentials required for the anodic reaction due to the sluggish kinetics of the oxygen evolution reaction (OER). Therefore, the development of more active and stable OER catalysts is crucial for the development and large-scale commercialization of this technology.

Earth-abundant elements are increasingly being investigated as OER catalysts in order to avoid the scarcity issues associated with catalysts based on platinum group metals (PGM).[1-3] Mixed transition metal oxides (perovskites and spinels) have shown a good intrinsic activity and in particular, the activity of bimetallic spinels has been extensively studied in the literature, mainly focusing on the determination of the active species toward OER.[4-8] However, less attention has been paid to the study of the durability of such electrocatalysts, which is measured as the performance loss during cycling treatments.[6,9] Recent studies have suggested an indirect relationship between the activity and stability of the materials. That is, the most active materials are generally the least stable.[9-11] If the catalyst experiences structural/chemical changes at the beginning of use, a significant evolution of the performance of the material will be expected after long-term operation. Therefore, the study of the durability becomes essential to establish the feasibility of these materials as OER catalysts. In this context, the use of advanced techniques that allow investigation of the materials under working (*operando*) conditions is especially important because they allow observation of both the reversible and irreversible changes experienced by the materials during the catalytic process, whereas the analysis of the samples after the catalytic work (*post-mortem*) can only show the irreversible ones.

In the study reported herein, we have prepared Co-Fe spinels of varying compositions and cation distributions. The Co-Fe oxides have been prepared both as *model* (ultrathin film) and *realistic* (powder) catalysts. Changes to the surfaces of the film were studied on the films by *in situ* X-ray photoemission spectroscopy (XPS), whereas surface/bulk transformations were investigated on powders by *operando* X-ray absorption spectroscopy (XAS) and *post-mortem* Mössbauer spectroscopy, transmission electron microscopy (TEM) and XPS. The pristine spinel structure as well as the cation distribution of the powders were determined by combining *ex situ* X-ray diffraction (XRD), Mössbauer spectroscopy and XAS. According to previously published studies of spinels, the geometric site (octahedral or

[a] Dipartimento di Scienze Chimiche, Università di Padova and INSTM Research Unit, Via Marzolo 1, 35131 Padova, Italia
[b] Dipartimento di Chimica Industriale "Toso Montanari", Università di Bologna, Viale Risorgimento 4, 40136 Bologna, Italia
[c] School of Chemistry, University of Bristol, Cantocks Close, BS8 1TS, Bristol, United Kingdom
[d] Istituto per l'Energetica e le Interfasi CNR-IENI and INSTM, Corso Stati Uniti, 4, 35127 Padova, Italia
[e] School of Chemistry, University of Southampton, Highfield, Southampton SO17 1BJ, UK
[f] Electron Microscopy Facility, Istituto Italiano di Tecnologia, Via Morego 30, 16163 Genova, Italia.
* E-mail: laura.calvillolamana@unipd.it, Tel.: +39 0498275122
§ Current address: UK Catalysis Hub, Research Complex at Harwell, RAL, Oxford, OX11 0FA, UK. And Kathleen Lonsdale Building, Department of Chemistry, University College London, Gordon Street, London, WC1H 0AJ, UK.
† Electronic Supplementary Information (ESI) available: [Synthesis of spinel films and powders, XPS, XRD, TEM and XAS characterization, and electrochemical characterization]. See DOI: 10.1039/x0xx00000x

tetrahedral) of the cations strongly influences their OER performance.[12-14] Changes in the structure and/or oxidation state of the cations can occur during the catalytic process, and these are expected to affect the activity of the materials. Our investigations have revealed that the surface of the Co-Fe spinels experiences an irreversible chemical and structural evolution under OER conditions, resulting in the formation of new Co(III) and Fe(III) species that have a crucial role in the activity loss of these materials.

2 Experimental

2.1 *In situ* X-ray Photoemission Spectroscopy (XPS) and Electrochemical Characterization

The preparation of the Co-Fe/Pd(100) systems, as well as the XPS analysis and the electrochemical characterization, was carried out in an ultrahigh vacuum (UHV) system already described in [15]. A brief description is found in the SI.
The chemical composition and structural changes induced by the electrochemical work were analysed by XPS. Photoemission data were obtained in a custom designed UHV system equipped with an EA 125 Omicron electron analyzer with five channeltrons, working at a base pressure of 10^{-9} mbar. Core level photoemission spectra (Pd 3d, Fe 2p, Co 2p and O 1s regions) were collected at room temperature with a non-monochromatized Al K_α X-ray source (1253.6 eV) using 0.1 eV energy steps, 0.5 s collection time and 20 eV pass energy.

A custom made PEEK (polyether ether ketone) cell, described in [15], was used for the electrochemical measurements. A Pt wire was used as counter electrode and an Ag/AgCl/Cl^-(3M KCl) electrode placed in a Luggin capillary was used as reference electrode. All the potentials reported in the text are referred to the reversible hydrogen electrode (RHE). The cell was controlled by an Autolab potentiostat running with NOVA 1.8 Software. The EC experiments were carried out in 0.1 M KOH, prepared from high purity reagents (Sigma-Aldrich). The electrolyte was pumped into the EC cell through a tubing system using a syringe pump (N-1010, Pump Systems Inc.), which allows an accurate control of the flow.

The films were characterized by cyclic voltammetry (CV) in order to determine the activity towards the OER. They were cycled between 0.8 V and 1.8 V vs RHE until the voltammogram was stable. Subsequently, the samples were analysed by XPS for determining the changes induced by the electrochemical work. All the electrochemical measurements were carried out at room temperature using a flow rate of 1 mL min^{-1}.

2.2 *Operando* X-ray absorption spectroscopy (XAS)

X-ray adsorption measurements were recorded on beamline B18 at Diamond Light Source (UK) with ring energy of 3 GeV and a current of 300 mA. The monochromator used was Si(311) crystals operating in Quick EXAFS (QEXAFS) mode. The operando measurements were carried out in fluorescence mode at the Co K (7709 eV) and Fe K (7112 eV) absorption edges at 298 K using a 36-element Ge detector. Calibration of the monochromator was carried out using the Co and Fe foils previously to the measurements. The acquired data was processed and analyzed using the Athena program.[16] An in situ electrochemical cell was used to collect XAS data of the Co-Fe spinels as a function of the applied potential. The working electrode was held in place by an Au wire contact, a Pt wire served as the counter electrode, and the reference electrode was a Hg/HgO electrode connected to the cell via a short length of tubing containing the electrolyte solution. The cell was controlled by an Autolab potentiostat running with NOVA 1.8 Software. The 0.1M KOH solution was pumped through the cell using a peristaltic pump. The samples were prepared as button electrodes (fresh electrodes) by painting Nafion-based inks onto carbon paper (TGP-H-60). The catalyst inks were prepared by dispersing the oxide and Vulcan XC-72 carbon powders (oxide:carbon mass ratio of 1:1) in a mixture of water and Na^+-exchanged Nafion® (5 wt.% solids in alcohol, Sigma-Aldrich). The electrodes were then pressed at 180 °C and 1 bar for 3 min. The XAS measurements were carried out at five different fixed potentials. Subsequently, the electrodes were subjected to an accelerated ageing treatment (AAT) (aged electrodes), which consisted of 1000 cycles between +1.35 V and +1.7 V vs RHE at 0.050 Vs^{-1}, in order to study the stability of the samples and, then, XAS measurements were performed at two fixed potentials (before and under OER condition). A linear scan voltammetry was run to reach the desired potential for the XAS measurements.

2.3 Mössbauer spectroscopy

Room Temperature Mössbauer spectroscopy was performed on a conventional constant acceleration spectrometer, with Rh matrix ^{57}Co source, nominal strength 1850 MBq. The hyperfine parameters isomer shift (δ), quadrupole shift (ε) and full linewidth at half maximum (Γ) are expressed in mms^{-1}, while internal magnetic field (B) is in Tesla and the relative area (A) in %. The parameters were obtained by means of standard least-squares minimization techniques.

2.4 Transmission electron microscopy (TEM)

TEM analyses were carried out with a FEI Tecnai F20 transmission electron microscope operated at 200 kV, using a single-tilt sample holder; whereas HAADF/EDS analyses were performed by using a JEOL JEM-2200FS transmission electron microscope operated at 200 kV and using a double-tilt analytical sample holder. The samples were prepared by dispersing them in ethanol and, subsequently, sonicating for 10 minutes. A drop of the sample solution was placed on a Cu grid, 150 mesh, coated with ultrathin amorphous carbon film. Before sample deposition each grid was plasma-treated (O_2+Ar plasma, 10 W, 2 minutes) in order to remove adsorbed hydrocarbons.

2.5 Durability study

Accelerated ageing tests (AAT) were performed in a conventional three-electrode electrochemical cell. An Ag/AgCl/Cl^- (KCl sat) electrode was used as reference electrode and a Pt wire as counter electrode. The potentials in this work have been converted to a reversible hydrogen electrode (RHE) reference electrode. Measurements were carried out in O_2-saturated 0.1 M KOH. A thin-film catalyst layer was deposited

on a glassy carbon (0.125 cm^2) electrode using a drop-casting method. 20 µL of ink containing 3 mg of Vulcan XC-72 carbon, 15 µL of Na^+-exchanged Nafion® (5 wt.%, Sigma-Aldrich) and 3 mg of the oxide catalyst were deposited on the glassy carbon disk. The electrodes were cycled between 1.35 V and 1.8 V at room temperature using a scan rate of 0.05 V s^{-1}. The evolution of the catalytic activity was determined by acquiring a CV between 1.0 V and 1.8 V after 250, 500 and 1000 cycles at 0.02 V s^{-1}.

3 Results and discussion

We have prepared three Co-Fe spinels ($Co_xFe_{3-x}O_4$, x = 0.6, 1, 2) with different composition: two cobalt ferrites ($Co_xFe_{3-x}O_4$, x = 0.6, 1) and an iron cobaltite ($FeCo_2O_4$). The samples were prepared both in form of powders (*realistic* catalysts) and ultrathin films (*model* catalysts). In the case of the as-prepared films, the structure and oxidation state of cations were determined by XPS (see Figure S1 of the supplementary information, SI). In the case of the as-prepared powders, however, the spinel structure and the morphology were already described in previous works,[17-18] and a brief summary can be found in Figures S2-S4 and Tables S1-S4.

After confirming the OER activity of the Co-Fe spinels (Figure S5), advanced *in situ* and *operando* methods were used to determine the chemical and/or structural changes induced under operating conditions. The changes induced on the Co-Fe oxide ultrathin films were determined by XPS. For the combined XPS/EC measurements, an UHV-EC transfer system that avoids any contact of the sample with air was used.[19] This tool allows identification of the changes produced only on the surface region, where the electrocatalytic reaction takes place. First, in order to facilitate the understanding of the changes caused by the electrochemical work, we discuss in detail the results obtained for ultrathin monometallic oxide films (CoO, Fe_3O_4 and Co_3O_4) and, subsequently, we analyze the results for the mixed Co-Fe systems.

Figure 1 shows the electrochemical results as well as the Co 2p and Fe 2p regions for the CoO, Co_3O_4 and Fe_3O_4 systems. The XPS analysis of the as-prepared ultrathin films confirmed the formation of the CoO and Fe_3O_4 phases on the Pd(100) substrate, as shown in Figures 1b and 1e.[20] CoO has a rock salt structure with the Co(II) ions occupying the octahedral (O_h) sites, whereas Fe_3O_4 presents an inverse spinel structure with Fe(II) atoms occupying the octahedral sites and Fe(III) both octahedral and tetrahedral (T_d) sites, as shown schematically in Figures 1c and 1f.[21]

The cyclic voltammograms (CVs) obtained at the CoO/Pd(100) surface showed an oxidation current starting at around 1.0 V in the first anodic sweep (Figure 1a). The following CVs, however, did not show oxidation currents in the 1.0 V – 1.5 V potential range, indicating an irreversible oxidation of the film during the first cycle. The XPS analysis after the electrochemical treatment confirmed the oxidation of the film leading to the formation of Co_3O_4. Therefore, the oxidation peak observed at potentials higher than 1.0 V is attributed to the oxidation of Co(II) to Co(III). In a previous work, where we studied ultrathin CoO films for the oxygen reduction reaction (ORR), we observed the total oxidation of CoO to Co_3O_4 (80 %) and CoOOH (20 %) in O_2-saturated 0.1 M KOH solution, even under less oxidative conditions (at 0.98 V vs RHE).[22] Therefore, the conversion of CoO into Co_3O_4 after the CVs between 1 V and 1.8 V is not surprising. Assuming that Co_3O_4 has a normal spinel structure at room temperature with Co(II) cations in T_d and Co(III) in O_h sites (Figure 1c),[23-24] it is deduced that both chemical and structural changes are induced on CoO under OER conditions.

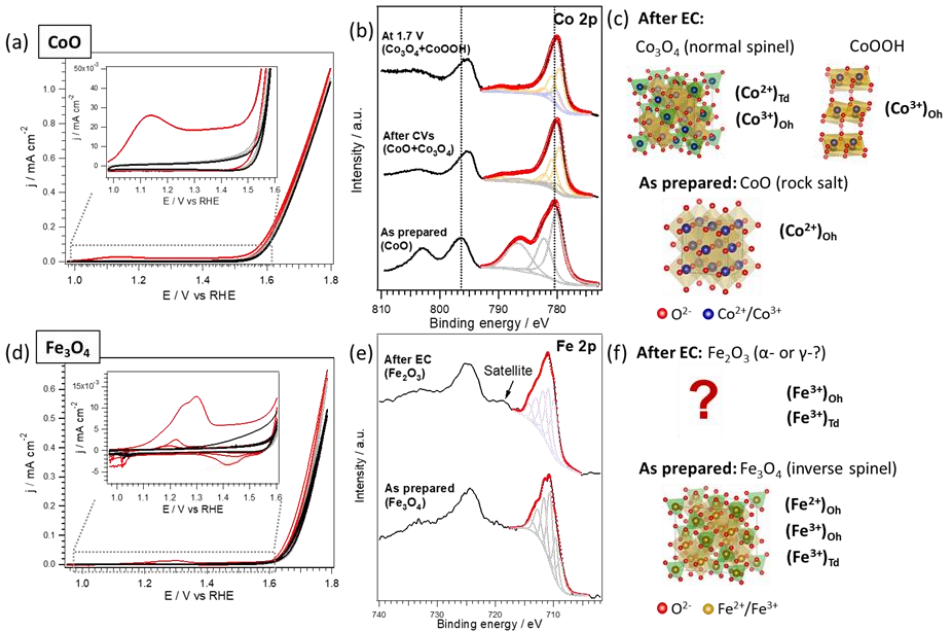

Fig. 1. Electrochemical, structural and chemical characterization of the films: cyclic voltammograms in 0.1 M KOH (a,d); Co 2p (b) and Fe 2p (e) XPS lines for the CoO and Fe_3O_4 film systems, respectively, before and after the electrochemical treatment; and proposed changes occurred during the electrochemical measurements (c,f). The insets in (a) and (d) show the redox peaks observed during the first cycles in more detail. Color code for Co and Fe species in (b) and (e): fresh samples (CoO and Fe_3O_4, grey), Co_3O_4 (yellow), CoOOH (blue), and Fe_2O_3 (purple).

Journal Name

ARTICLE

After obtaining the Co_3O_4/Pd(100) system through oxidation of CoO/Pd(100), we polarized the system at 1.7 V (OER conditions) for 30 min in order to investigate a further evolution of the sample under catalytic conditions. The results show that the complete oxidation of the residual CoO into Co_3O_4 and that the partial conversion of the Co_3O_4 to CoOOH occurs under these conditions (top panel in Figure 1b). Therefore, a further chemical evolution of the systems takes places under catalytic conditions. In the literature, the *in situ* formation of CoOOH under OER conditions has been already observed and identified as the real active phase for this reaction.[14,25,26] In addition, the fact that Co_3O_4 is only partially transformed into CoOOH has been recently reported by Favaro et al..[25] Regarding the structural changes, it can be assumed that restructuring of the surface also takes place in this case, considering that Co(III) occupies the O_h sites in CoOOH and, most probably, only the Co(II) species in T_d site are able to undergo this transformation.[26]

For the Fe_3O_4/Pd(100) system, redox peaks associated with the Fe(II)/Fe(III) redox couple were observed during the first cycle, whose intensity gradually decreased in the following scans (Figure 1d). After the third cycle, these processes became negligible and the CVs stable, indicating that an irreversible oxidation of the film occurred. The XPS analysis of this sample confirmed that a chemical change took place during the cycling treatment, in particular the oxidation of Fe_3O_4 to Fe_2O_3. This change is clearly evidenced by the appearance of the Fe $2p_{3/2}$ satellite peak at 718.7 eV, characteristic of Fe_2O_3.[27] Recently, it has been reported in the literature that FeOOH is not formed on the surface of Fe_3O_4, which has been attributed to the atomic mismatch of the different structures of FeOOH and Fe_3O_4.[26] Regarding the structural variation, unfortunately in this case, it is not possible to determine it with precision, since XPS measurements cannot distinguish between α-Fe_2O_3 and γ-Fe_2O_3.

The same study was performed on the Co-Fe mixed oxides films and the results are reported in Figures S5 and S6. When analyzing the XPS data of mixed Co-Fe systems, however, the overlapping of the Fe LMM and Co LMM lines and the Co 2p and Fe 2p regions makes difficult their interpretation. The *in situ* XPS/EC measurements performed on these mixed systems suggest that the phase with a greater amount of Co (cobaltite phase) is oxidized under OER conditions leading to the formation of Co_3O_4, although the formation of CoOOH cannot be excluded. As a consequence of the Co oxidation and formation of new Co(III) species, a change in the coordination of the Fe atoms is expected, forming Fe_2O_3 as seen above due to the oxidative working conditions. In contrast, the phases with higher content of Fe (ferrite phases) are very stable under OER conditions with only a slight oxidation of Co(II) to Co(III).

The chemical and structural changes experienced by the fresh and aged powder materials were investigated by *operando* XAS. For each fresh material, five different potentials, increasing from 1.0 up to 1.7 V_{RHE} (1.0, 1.2, 1.4, 1.6 and 1.7 V), were studied in order to determine the changes in the oxidation state and coordination environment with the applied potential at the Fe K and Co K edges. Aged electrodes were only studied at two different potentials, before (1.2 V) and under OER conditions (1.7 V). Figures 2 and 3 display the X-ray absorption near-edge structure (XANES) and Fourier transform (FT) extended X-ray absorption fine structure (EXAFS) data at the Fe K and Co K edges, respectively. Changes in the XANES and FT EXAFS spectra with the applied potential were observed for the $FeCo_2O_4$ sample at both Fe K and Co K edges, whereas no variations were discerned for the cobalt ferrite samples.

The XANES region for the $FeCo_2O_4$ spinel shows a gradual shift towards higher energy values at both the Fe K and Co K edges when the potential increased from 1.0 to 1.7 V (Figure S7), indicating an increase of the both Co and Fe oxidation states. It is supposed that only the surface Co and Fe cations are oxidized, while the bulk remains unchanged. For this reason, only small changes are observed. Taking into account the Co and Fe oxidation states of the fresh sample (Figure S3), it is clear that the changes observed correspond to the oxidation of Co(II) and Fe(II) to Co(III) and Fe(III), respectively. In addition, a gradual decrease of the pre-edge peak and an increase of the intensity of the post-edge peak were observed when the applied potential increased. The intensity and position of the pre-edge peak are sensitive not only to the oxidation state of the metal but also to the degree of symmetry around it. Thus, non-centrosymetric T_d metal environments present more intense pre-peak features than centrosymmetric O_h ones.[28,29] Therefore, the variation in intensity of the pre-edge and the post-edge peak are associated with changes in the chemical environment of the absorber atom. In our case, the trends observed are attributed to a decrease of tetrahedrally coordinated Co and Fe cations and an accompanying increase of Co and Fe cations in O_h sites.[30]

In order to interpret the XAS data, the results obtained from the *model* systems were considered. The increase of Co(III) species in O_h site is in agreement with the formation of Co_3O_4 and CoOOH observed for the ultrathin films. As described above, Co_3O_4 is formed by Co(II) cations in T_d sites and Co(III) in O_h sites, while CoOOH only contains Co(III) in O_h sites (Figure 1c). As observed for the *model* systems, CoOOH is only formed under OER conditions. Therefore, the gradual oxidation of cobalt, even under pre-catalytic conditions, could be interpreted as an initial oxidation of $Co(II)_{T_d}$ to Co_3O_4 under pre-catalytic conditions with a further conversion into CoOOH under catalytic conditions, which has been identified as catalytic OER

phase.[14,25,26,31] Similarly, the increase of Fe(III) in O_h sites is in agreement with the conversion of $Fe(II)_{T_d}$ into Fe_2O_3. The formation of Fe_2O_3 would be the consequence of the Co species evolution under pre- and catalytic conditions. That is, if the Co cations of the Co-Fe spinel are oxidized forming new Co phases, a spinel structure with an excess of Fe will be obtained, favouring the formation of the more stable Fe_2O_3 phase. However, a simple oxidation due to the oxidative operation conditions (presence of oxygen and high potentials) cannot be excluded.

These changes are also supported by the variations observed in the Fourier transforms of the EXAFS spectra at both the Co K and Fe K edges. A slight compression in the Co-O and Fe-O bonds occurs with the increase of the applied potential, which is in agreement with the formation of Co_3O_4/CoOOH and Fe_2O_3, respectively.[31]

The analysis of the aged samples showed that these changes become more significant with cycling and become independent of the potential applied during the measurement of the XAS. This suggests that the changes observed are related to an irreversible modification of the catalyst surface and not just to the *in situ* formation of active sites. In the literature, it has been reported that these changes are reversible, stating the formation of an amorphous $CoO_x(OH)_y$ shell on Co_3O_4 under OER catalytic conditions and its re-crystallization upon return to non-catalytic conditions.[32] However, our results clearly show that the changes experienced by $FeCo_2O_4$ under OER conditions are irreversible.

To further investigate and confirm the surface transformation experienced by the $FeCo_2O_4$ powder catalyst during the OER process, *post-mortem* analysis were performed by using Mössbauer spectroscopy, XPS and TEM. Figure 4a reports the Mössbauer spectra for the fresh and aged samples. Both spectra show a broad magnetic pattern as a result of the magnetic relaxation due to high ordering temperature.[18,33] No substantial changes are observed in the spectrum after the cycling treatment, compared to that of the fresh sample, confirming the bulk stability of the material. In contrast, the analysis of the XPS Co 2p region shows that the Co $2p_{3/2}$ peak shifts slightly to lower BE and becomes narrower (Figure 4b). In addition, the spin orbit splitting decreases from 15.4 eV to 14.8 eV after the cycling treatment, as observed for the thin films in Figure 1b.[21] These effects are indicators of the increase of Co(III) in the surface of the aged sample, which is again in agreement with the formation of Co_3O_4/CoOOH phases.

TEM images of the aged sample showed the formation of an about 3 nm thick amorphous layer at the surface of the nanoparticles, while the bulk remained unaltered (Figures 4c, 4d and S8). This layer would be in good agreement and could be associated with the formation of Co_3O_4, CoOOH and Fe_2O_3 species, as seen from XAS and XPS. The atomic rearrangement of the surface for iron spinels has been recently reported by Hsu *et al.*.[26] They demonstrated that this rearrangement resulted in the formation of the metal oxyhydroxides, but it only occurs for cobalt and nickel and not for iron and zinc ferrites. This result also justifies the fact that we did not observe the formation of FeOOH. On the other hand, similar studies on perovskite oxides have demonstrated that the surface amorphization occurs also for these oxides under OER conditions.[11,34] May *et al.* observed a quick amorphization of the $Ba_{0.5}Sr_{0.5}Co_{0.8}Fe_{0.2}O_{3-\delta}$ surface under OER in alkaline conditions and the selective leaching of Ba^{2+} and Sr^{2+} ions. However, they did not identify the Co and Fe phases formed on the surface. More recently, Fabbri *et al.* also reported the creation of an amorphous surface layer on $Ba_{0.5}Sr_{0.5}Co_{0.8}Fe_{0.2}O_{3-\delta}$.[11] In this case, the authors claimed that this layer was composed of CoOOH and FeOOH, and proposed a mechanistic model for its formation based on thermodynamic calculations.[35]

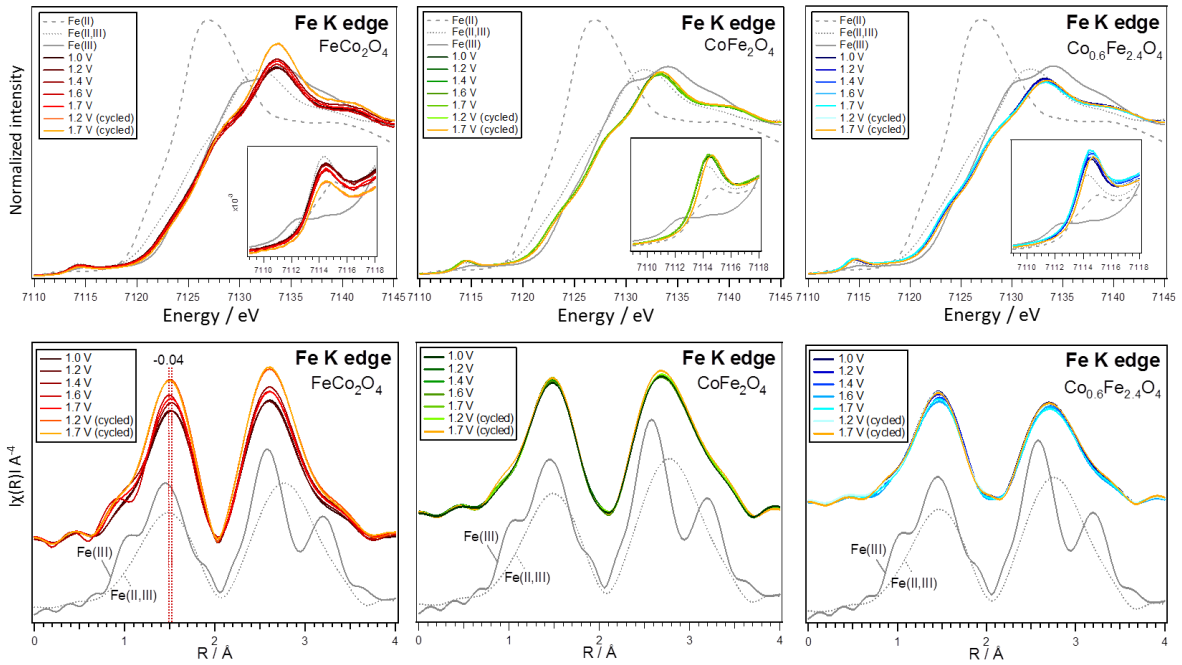

Fig. 2. *Operando* XAS characterization of the powders: XANES (upper panels) and FT EXAFS (bottom panels) spectra at Fe K edge for the fresh and aged $FeCo_2O_4$ (red), $CoFe_2O_4$ (green) and $Co_{0.6}Fe_{2.4}O_4$ (blue) spinels recorded at different applied potentials in 0.1 M KOH at room temperature. The inset in the upper panels corresponds to the zoom of the pre-edge peak.

Journal Name

ARTICLE

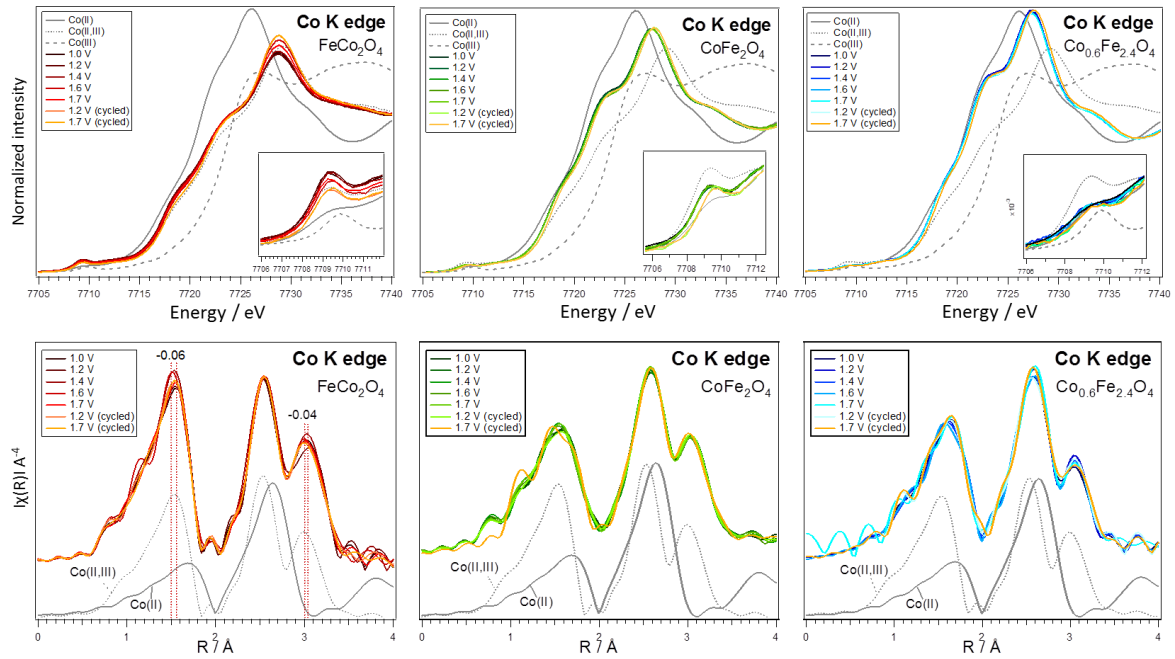

Fig. 3. *Operando* XAS characterization of the powders: XANES (upper panels) and Fourier transformed EXAFS (bottom panels) spectra at Co K edge for the fresh and aged $FeCo_2O_4$ (red), $CoFe_2O_4$ (green) and $Co_{0.6}Fe_{2.4}O_4$ (blue) spinels recorded at different applied potentials in 0.1 M KOH at room temperature. The inset in the upper panels corresponds to the zoom of the pre-edge peak.

Even if many similarities can be found in the changes experienced by spinel and perovskite oxides, noteworthy differences are apparent as well: (i) spinel oxides undergo chemical/structural changes already at pre-catalytic OER conditions and become more significant under OER conditions, while the changes suffered by perovskite oxides have only been detected under OER catalytic conditions; (ii) A-site elements dissolution takes place under operation conditions in perovskite structures while, in our case, the energy dispersive spectroscopy (EDS) analysis of the fresh and aged sample did not show any evidence of a selective leaching of iron or cobalt (Figure S9). The average atomic Co/Fe ratio for the fresh sample was determined as 1.8 ± 0.2, whereas that for the aged sample was 2.0 ± 0.2. Therefore, the differences observed are within the error. This result is further confirmed by XPS. The surface Co:Fe atomic ratio was calculated from photoemission spectra for fresh and aged samples taking into account the corresponding sensitivity factors. The calculated Co:Fe ratio resulted to be 67:33 and 68:32 for the fresh and aged sample, respectively. This value agrees well with the nominal stoichiometry (Co_2FeO_4) and confirms that there is no preferential leaching of any of the cations.

For the $Co_xFe_{3-x}O_4$ (x = 0.6, 1) samples, unlike for $FeCo_2O_4$, the analysis of the XANES and EXAFS regions did not show changes in the spectra at the Co K or Fe K edges with the applied potential. Nevertheless, also in this case, an irreversible surface chemical oxidation on the aged samples was observed, evidenced by the slight shift of the edge and pre-edge towards higher energies (Figures 2 and S8). The fact that no changes were observed for these samples can be explained by taking into account the composition and cation distribution of the three Co-Fe spinels. As seen for $FeCo_2O_4$, the cobalt species that experience an evolution under working conditions are Co(II) cations occupying T_d sites. The fraction of $Co(II)_{T_d}$ species in $FeCo_2O_4$ is much higher than in $CoFe_2O_4$ and is almost negligible in $Co_{0.6}Fe_{2.4}O_4$ (Table S1). For this reason, only significant changes are observed for $FeCo_2O_4$. It should be highlighted that the fact that a smaller fraction of the Co and Fe atoms change the chemical environment during operating conditions, compared to the $FeCo_2O_4$ spinel, cannot be attributed to a particle size effect, since the particle size of the $FeCo_2O_4$ sample is larger than that of $Co_xFe_{3-x}O_4$ (x = 0.6, 1), as seen by TEM and XRD (Figure S2). Therefore, the results show that ferrites are more chemically stable than cobaltite under OER conditions.

The irreversible changes experienced by the oxides under OER conditions determine their durability. Figure 5 shows the evolution of the OER activity during the accelerated stability tests. A progressive loss of the initial activity was observed for all samples with the number of cycles, except for Co_3O_4 that

showed a very stable performance. The high durability of Co_3O_4 can be attributed to its high chemical and structural stability under OER conditions, as seen from *in situ* XPS/EC measurements. In the case of the Co-Fe spinels, however, the chemical and structural changes occurring during the long-term operation can be related to the different degree of activity loss of these materials: a higher activity loss is observed for $CoFe_2O_4$ than for $FeCo_2O_4$. The majority cations in these samples are Fe and Co, respectively; therefore, Fe_2O_3 will be preferentially formed on the surface of $CoFe_2O_4$, whereas Co_3O_4/CoOOH will be formed on $FeCo_2O_4$. From the results obtained for Co_3O_4 and Fe_3O_4, used as reference, it is deduced that Co_3O_4 is catalytically active and stable, whereas Fe_3O_4 is not very active or stable, being the one with a higher activity loss. The higher activity loss can be attributed to the formation of Fe_2O_3 as it has minimal OER activity.[26] Therefore, the preferential formation of Co_3O_4/CoOOH on the surface will not cause a significant activity loss, as observed for $FeCo_2O_4$, while a preferential formation of Fe_2O_3 will lead to a higher activity loss as it happens for $CoFe_2O_4$.

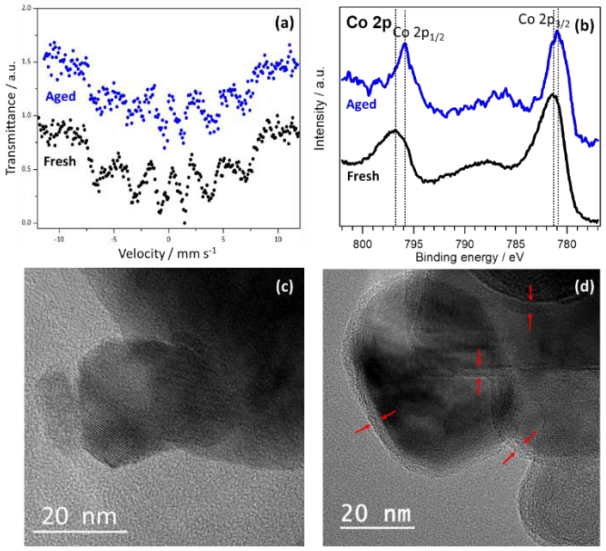

Fig. 4. *Post-mortem* characterization of the $FeCo_2O_4$ powder: Mössbauer spectra acquired at room temperature (a); Co 2p XPS region (b); and TEM images of the as-prepared (c) and aged (d) samples. The red arrows in (d) point out the amorphous layer.

In a previous work, Kargar *et al*. studied the durability of $CoFe_2O_4$ NPs, observing the decrease of the current density as the number of cycles increased. The *post-mortem* analysis of the sample by SEM and XRD did not show any morphological or chemical change in the material; therefore, they attributed the activity loss to the formation of bubbles during the experiment.[6] In this work, however, we have shown that an irreversible oxidation of the surface of the $CoFe_2O_4$ nanoparticles occurs under OER conditions, which is responsible for the long-term activity loss. The changes experienced by this material under catalytic conditions cannot be determined by SEM or XRD, since they are not sensitive to surface chemical variations. Therefore, this result confirms that the combination of surface and bulk sensitive techniques under *in situ/operando* conditions is crucial to establish structural/activity/durability relationships. The understanding of the modifications that the materials experience during the catalytic process can be the key for the design of highly active and durable catalysts

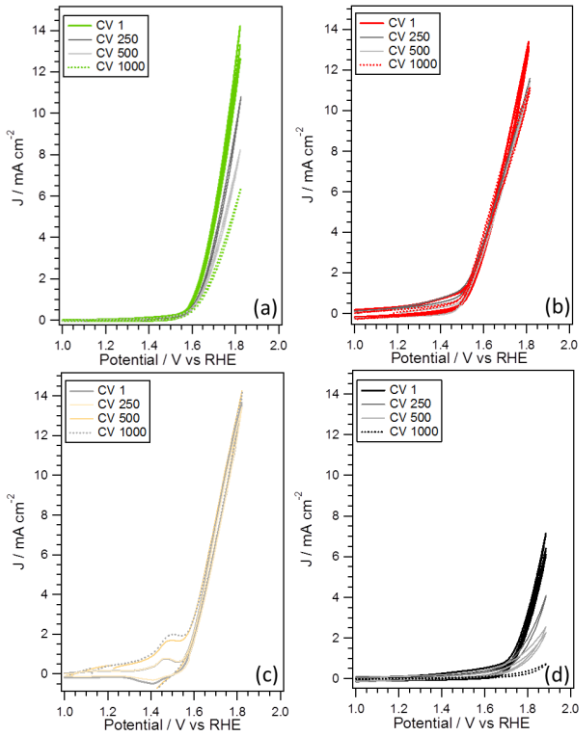

Fig. 5. Study of durability. CVs (not IR-corrected) after 1, 250, 500 and 1000 potential cycles for the $CoFe_2O_4$ (a), $FeCo_2O_4$ (b), Co_3O_4 (c), and Fe_3O_4 (d) powder samples. All the measurements were performed in O_2-saturated 0.1 M KOH at room temperature.

4 Conclusions

Co-Fe spinels ($Co_xFe_{3-x}O_4$, x = 0.6, 1, 2) were prepared both as *model* (ultrathin film) and *realistic* (powder) catalysts. Subsequently, the chemical and structural changes experienced during the OER process were investigated by using *in situ* XPS, *operando* XAS and *post-mortem* Mössbauer spectroscopy, XPS and TEM. This approach allowed determination of the transformations undergone both at the surface and in the bulk of the spinel oxides, which were then related to the OER durability.

The three bimetallic Co-Fe spinel samples suffered irreversible oxidation under OER conditions leading to the formation of a layer consisting of Co_3O_4, CoOOH and Fe_2O_3. The extension of this oxidation depended on the composition and cation distribution of the spinel oxides, since the Co(II) cations in T_d sites were those that experienced the modifications. Thus, the two cobalt ferrites were shown to be stable under working conditions, presenting only a slight oxidation of the surface, whereas the iron cobaltite suffered a significant modification. However, we found that the durability does not depend simply on the chemical stability but on the identity of the new species formed. Thus, iron cobaltite showed the lowest performance loss, which can be attributed to the preferential formation of Co_3O_4 and CoOOH, which is stable and actually is the active phase. In the case of the cobalt ferrites, the preferential formation of Fe_2O_3, which is a less active OER catalyst, was accompanied by a greater loss of activity.

Conflicts of interest

There are no conflicts to declare.

Acknowledgements

G.G., L.C. and S.A. acknowledge the Italian Minister of University (MIUR) for financial support to the SMARTNESS project financed thorough the grant: PRIN 2015K7FZLH. V.C. and D.J.F. kindly acknowledge the UK Catalysis Hub for resources and support provided via the membership of the UK Catalysis Hub Consortium and funded by EPSRC (EPSRC grants EP/K014706/1 and EP/K014714/1). Preliminary TEM studies were carried out at the University of Bristol Chemistry Imaging Facility with equipment funded by UoB and EPSRC (EP/K035746/1 and EP/M028216/1). The authors wish to acknowledge the Diamond Light Source for provision of beamtime (SP12835), and Dr Giannantonio Cibin is acknowledged for the excellent beamline support.

References

1 M. S.Burke, L. J. Enman, A. S. Batchellor, S. Zou and S. W. Boettcher. *Chem. Mater*. 2015, **27**, 7549−7558.
2 J. Chang, Y. Xiao, M. Xiao, J. Ge, Ch. Liu and W. Xing. *ACS Catal*. 2015, **5**, 6874−6878.
3 F. Dionigi and P. Strasser. *Adv. Energy Mater*. 2016, **6**, 1600621.
4 K. Chakrapani, G. Bendt, H. Hajiyani, I. Schwarzrock, T. Lunkenbein, S. Salamon, J. Landers, H. Wende, R. Schlögl, R. Pentcheva, M. Behrens and S. Schulz. *ChemCatChem* 2017, **9**, 2988-2995.
5 Y. Liu, J. Li, F. Li, W. Li, H. Yang, X. Zhang, Y. Liu and J. Ma. *J. Mater. Chem. A*, 2016, **4**, 4472-4478.
6 A. Kargar, S. Yavuz, T. K. Kim, Ch.-H. Liu, C. Kuru, C. S. Rustomji, S. Jin, P. R. Bandaru. *ACS Appl. Mater. Interfaces* 2015, **7**, 17851−17856.
7 X.-F. Lu, L.-F. Gu, J.-W. Wang, J.-X. Wu, P.-Q. Liao and G.-R. Li. *Adv. Mater*. 2017, **29**, 1604437.
8 W. Bian, Z. Yang, P. Strasser and R. A Yang. *J. Power Sources* 2014, **250**, 196-203.
9 S. H. Chang, N. Danilovic, K.-Ch. Chang, R. Subbaraman, A. P. Paulikas, D. D. Fong, M. J. Highland, P. M. Baldo, V. R. Stamenkovic, J. W. Freeland, J. A. Eastman and N. M. Markovic. *Nat. Commun*. 2014, **5**, 4191.
10 N. Danilovic, R. Subbaraman, K.-Ch. Chang, S. H. Chang, Y. J. Kang, J. Snyder, A. P. Paulikas, D. Strmcnik, Y.-T. Kim, D. Myers, V. R. Stamenkovic and N. M. Markovic. *J. Phys. Chem. Lett.* 2014, **5**, 2474−2478.
11 E. Fabbri, M. Nachtegaal, T. Binninger, X. Cheng, B.-J. Kim, J. Durst, F. Bozza, T. Graule, R. Schäublin, L. Wiles, M. Pertoso, N. Danilovic, K. E. Ayers and T. J. Schmidt. *Nat. Mater.* 2017, DOI: 10.1038/NMAT4938.
12 H.-Y. Wang, S.-F. Hung, H.-Y. Chen, T.-S. Chan, H. M. Chen and B. Liu. *J. Am. Chem. Soc.* 2016, **138**, 36-39.
13 C. Schwanke, H. S. Stein, L. Xi, K. Sliozberg, W. Schuhmann, A. Ludwig and K. M. Lange. *Sci Rep*. 2017, **7**, 44192.
14 X. Wang, Y. Liu, T. Zhang, Y. Luo, Z. Lan, K. Zhang, J. Zuo, L. Jiang and R. Wang. *ACS Catal*. 2017, **7**, 1626−1636.
15 L. Calvillo, D. Fittipaldi, C. Rüdiger, S. Agnoli, M. Favaro, C. Valero-Vidal, C. Di Valentin, A. Vittadini, N. Bozzolo, S. Jacomet, L. Gregoratti, J. Kunze-Liebhäuser, G. Pacchioni and G. Granozzi. *J. Phys. Chem. C* **2014**, *118*, 22601-22610.
16 B. Ravel and M. J. Newville. *Synchrotron Rad*., 2005, *12*, 537.
17 O. Vozniuk, S. Agnoli, L. Artiglia, A. Vassoi, N. Tanchoux, F. Di Renzo, G. Granozzi and F. Cavani. *Green Chem*. 2016, **18**, 1038-1050.
18 F. Carraro, O. Vozniuk, L. Calvillo, L. Nodari, C. La Fontaine, F. Cavani, S. Agnoli. *J. Mater. Chem. A*, 2017, DOI: 10.1039/c7ta06785b.
19 L. Calvillo, G. García, A. Paduano, O. Guillen-Villafuerte, C. Valero-Vidal, A. Vittadini, M. Bellini, A. Lavacchi, S. Agnoli, A. Martucci, J. Kunze-Liebhäuser, E. Pastor and G. Granozzi. *ACS Appl. Mater. Interfaces* 2015, **8**, 716-725.
20 M. C. Biesinger, B. P. Payne, A. P. Grosvenor, L. W. M. Lau, A. R. Gerson and R.St.C. Smart, *Appl. Surf. Sci.* 2011, **257**, 2717–2730.
21 Q. Zhao, Z. Yan, C. Chen and J. Chen. *Chem. Rev.* 2017, **117**, 10121-10211.
22 T. Kosmala, L. Calvillo, S. Agnoli and G. Granozzi. *ACS catalysis* 2018, **8**, 2343–2352.
23 L. Bai, M. Pravica, Y. Zhao, C. Park, Y. Meng, S. V. Sinogeikin and G. Shen. *J. Phys.: Condens. Matter* 2012, **24**, 435401-435407.
24 J. Chen and A. Selloni. *Phys. Rev. B,* 2012, **85**, 085306.
25 M. Favaro, J. Yang, S. Nappini, E. Magnano, F. M. Toma, E. J. Crumlin, J. Yano and I. D. Sharp. *J. Am. Chem. Soc*. 2017, **139**, 8960–8970.
26 C.-S. Hsu, N.-T. Suen, Y.-Y. Hsu, H.-Y. Lin, C.-W. Tung, Y.-F. Liao, T.-S. Chan, H.-S. Sheu, S.-Y. Chen and H. M. Chen. *Phys.Chem.Chem.Phys*., 2017, **19**, 8681-8693.
27 T. Yamashita and P. Hayes. *Appl. Surf. Sci*. 2008, **254**, 2441–2449.
28 M. H. Nilsen, C. Nordhei, A. L. Ramstad, D. G. Nicholson, M. Poliakoff and A. Cabañas. *J. Phys. Chem. C,* 2007, **111**, 6252-6266.
29 F. De Groot, G. Vankó and P. Glatzel. *J. Phys.: Condens. Matter* 2009, **21**, 104207.
30 S. J. Stewart, S. J. A. Figueroa, J. M. Ramallo López, S. G. Marchetti, J. F. Bengoa, R. J. Prado and F. G. Requejo. *Phys. Rev. B* 2007, **75**, 073408.
31 B. Seo, Y. J. Sa, J. Woo, K. Kwon, J. Park, T. J. Shin, H. Y. Jeong and S. H. Joo. *ACS Catal*. 2016, **6**, 4347−4355.
32 A. Bergmann, E. Martinez-Moreno, D. Teschner, P. Chernev, M. Gliech, J. Ferreira de Araujo, T. Reier, H. Dau and P. Strasser. *Nat. Commun*. 2015, **6**, 8625.
33 T. A. S. Ferreira, J. C. Waerenborgh, M. H. R. M. Mendonça, M. R. Nunes and F. M. Costa *Solid State Sci*., 2003, **5**, 383–392.
34 K. J. May, C. E. Carlton, K. A. Stoerzinger, M. Risch, J. Suntivich, Y.-L. Lee, A. Grimaud, Y. Shao-Horn. *J. Phys. Chem. Lett*. 2012, **3**, 3264−3270.
35 T. Binninger, R. Mohamed, K. Waltar, E. Fabbri, P. Levecque, R. Kötz, T. J. Schmidt. *Sci. Rep.* 2015, **5**, 12167.

